Subdomain Structures of Lamellar and Reverse Hexagonal Pluronic Ternary Systems Investigated by Small Angle Neutron Scattering

Changwoo Doe,[†] Hyung-Sik Jang,[†] Steven R. Kline,[‡] and Sung-Min Choi*,[†]

Department of Nuclear and Quantum Engineering, Korea Advanced Institute of Science and Technology, 373-1 Guseong-dong, Yuseong-gu, Daejeon, 305-701, Republic of Korea, NIST Center for Neutron Research, Gaithersburg, Maryland 20899-6102

Received October 13, 2008; Revised Manuscript Received February 6, 2009

ABSTRACT: The subdomain structures of lamellar and reverse hexagonal phases of P84/water/*p*-xylene ternary system have been investigated by contrast varied small angle neutron scattering (SANS) measurements. As the neutron scattering length density of either polar or apolar domain was varied, the scattering intensities of the first Bragg peaks changed as expected, but the intensities of the second Bragg peaks did not change significantly. This variation of the relative peak intensities can not be explained by the typical simple models where the polar and apolar domains are regarded as homogeneous mixtures of PEO + water and PPO + oil, respectively, in which case the relative intensities of Bragg peaks do not change. For both lamellar and reverse hexagonal Pluronic ternary systems, the analysis of the contrast varied SANS intensities with subdomain structure models reproduce the experimental data very successfully, showing that a water-rich layer exists in the middle of the polar domain and water- and oil-depleted layers exist at the polar/apolar interfaces.

Introduction

Poly(ethylene oxide)−poly(propylene oxide)−poly(ethylene oxide) (PEO−PPO−PEO) triblock copolymers in water and oil mixture exist in various phases such as micellar, lamellar, and hexagonal phases[1−4] and have been of great interest to researchers for their wide range of applications including templates for various nanostructures[5−7] and nanoparticles[8−13] to pharmaceutics.[14−16] The isothermal phase behavior of various PEO−PPO−PEO block copolymers in water and oil solvents, which depends on the PEO/PPO block ratio, molecular weight, solvent type, and the compositions of mixtures, has been studied extensively[1−3,17−20] where small-angle neutron scattering (SANS) and small-angle X-ray scattering (SAXS) techniques have been generally used. In most studies, the PEO and PPO blocks are assumed to be homogeneously distributed within water and oil,[21,22] respectively, forming polar and apolar regions. This works quite well assigning the peak positions of scattering intensities corresponding to relevant structures. However, the detailed local structures of polar and apolar domains of the PEO−PPO−PEO block copolymer ternary systems, which, together with the scattering contrasts, determine the relative intensities of scattering peaks, have not been fully explored yet. It is expected that the detailed local structures of polar and apolar domains will not only provide better understanding of the ternary systems but also provide critical information for the size- and shape-controlled fabrication of various nanoparticles and nanostructures where the PEO−PPO−PEO block copolymer ternary systems are used as templates.

In this study, we have investigated the local domain structures of lamellar and reverse hexagonal phases formed by a Pluronic P84 ($(EO)_{19}(PO)_{43}(EO)_{19}$) block copolymer/water/*p*-xylene ternary system[3] by contrast varied small angle neutron scattering (SANS) measurements. Simultaneous analysis of a series of contrast varied scattering intensities of the ternary systems at lamellar and reverse hexagonal phases, respectively will allow us to determine the detailed local structures of polar and apolar domains. To our knowledge, this is the first experimental study to elucidate the detailed local structures of polar and apolar domains of ternary Pluronic systems.

Experimental Section

Materials. The Pluronic P84, $(EO)_{19}(PO)_{43}(EO)_{19}$, block copolymer was provided by BASF as a gift and was used as received. Deionized water (Milli-Q, Millipore) was used for hydrogenated water (H_2O). Hydrogenated *p*-xylene of purity >99% was purchased from Sigma-Aldrich. Deuterated water (D_2O, 99.9 atom % D) and deuterated *p*-xylene ($C_6D_4(CD_3)_2$, > 98 atom % D) were purchased from Cambridge Isotope Laboratories. Samples were prepared using the previously known phase diagram at 25 °C.[3] Lamellar phase samples were prepared at a composition of P84/water/*p*-xylene of 40/40/20 ratio by mass. For reverse hexagonal phase samples, the P84/water/*p*-xylene mass ratio was 46/18/36. The samples were centrifuged repeatedly in alternating directions for several days to facilitate homogeneous mixing, and kept at room temperature.

Contrast Varied Small-Angle Neutron Scattering Measurements. SANS measurements were performed on the NG7 30m SANS instrument at the National Institute of Standards and Technology (NIST) in Gaithersburg, MD.[23] Neutrons of wavelength $\lambda = 6$ Å with full width half-maximum $\Delta\lambda/\lambda = 11\%$ were used. The sample to detector distance of 4 m was used to cover the overall q range of 0.012 Å$^{-1} < q < 0.152$ Å^{-1} where $q = (4\pi/\lambda)\sin(\theta/2)$ is the magnitude of the scattering vector and θ is the scattering angle. Sample scattering was corrected for background and empty cell scattering, and the sensitivity of individual detector pixels. The corrected data sets were placed on an absolute scale using the data reduction software provided by NIST[24] through the direct beam flux method. All the SANS measurements were carried out at 25 °C using quartz cells of 1 mm path length. The mixing ratio of hydrogenated and deuterated solvents (water and *p*-xylene) was varied to control the neutron scattering contrasts of either the polar or apolar domains. The scattering length densities (SLD) of PEO,[25] PPO,[25] H_2O, D_2O, *p*-xylene, and *p*-xylene-d_{10} are 0.57, 0.35, −0.57, 6.33, 0.77, and 5.84×10^{10} cm^{-2}, respectively.

For lamellar phase samples, while the SLD of oil was kept constant by using deuterated *p*-xylene, the SLD of water was varied by using mixtures of H_2O and D_2O with different H_2O weight fractions (0, 10, 20, 30, 40, 50, and 60 wt %). If we assume that the polar and apolar regions are homogeneous mixtures of PEO + water and PPO + oil, respectively, the averaged apolar domain

* Corresponding author. E-mail: sungmin@kaist.ac.kr.
[†] Department of Nuclear and Quantum Engineering, Korea Advanced Institute of Science and Technology.
[‡] NIST Center for Neutron Research.

10.1021/ma802296u CCC: $40.75 © 2009 American Chemical Society
Published on Web 03/19/2009

Table 1. SLDs of solvents (water ρ_w and oil ρ_o), averaged polar domain ($\bar{\rho}_{polar}$), and average apolar domain ($\bar{\rho}_{apolar}$) at given weight fractions of hydrogenated solvents. The unit of SLD is $\times 10^{10}$ cm^{-2}

lamellar phase				reverse hexagonal phase			
H_2O wt %	ρ_w	$\bar{\rho}_{polar}$	$\bar{\rho}_{apolar}$	*p*-xylene wt %	ρ_o	$\bar{\rho}_{polar}$	$\bar{\rho}_{apolar}$
0	6.33	4.63	3.00	0	5.84	3.34	3.61
10	5.58	4.11	3.00	3	5.67	3.34	3.51
20	4.84	3.59	3.00	6	5.50	3.34	3.41
30	4.12	3.09	3.00	9	5.35	3.34	3.32
40	3.41	2.59	3.00	12	5.17	3.34	3.23
50	2.72	2.10	3.00	15	5.02	3.34	3.14
60	2.03	1.62	3.00				

SLD is calculated to be $\bar{\rho}_{apolar} = 3.00 \times 10^{10}$cm^{-2} while the averaged polar domain SLD ($\bar{\rho}_{polar}$) varies from 4.63×10^{10} cm^{-2} to 1.62×10^{10} cm^{-2} as the weight fraction of the hydrogenated water changes from (0 to 60) wt % (Table 1). The lowest scattering intensity is expected when the weight fraction of H_2O is 30 wt %.

For reverse hexagonal phase samples, the SLD of water was kept constant by using D_2O and the SLD of oil was varied by using mixtures of hydrogenated and deuterated *p*-xylene with different hydrogenated *p*-xylene weight fractions (0, 3, 6, 9, 12, 15 wt %). Here, if we assume homogeneous mixtures of PEO + water and PPO + oil for the polar and apolar regions, respectively, the averaged polar domain SLD is calculated to be $\bar{\rho}_{polar} = 3.34 \times 10^{10}$cm^{-2} and the averaged apolar domain SLD ($\bar{\rho}_{apolar}$) varies from 3.61×10^{10} cm^{-2} to 3.14×10^{10} cm^{-2} as the weight fraction of the hydrogenated *p*-xylene changes from (0 to 15) wt % (Table 1). The lowest scattering intensity is expected when the weight fraction of hydrogenated *p*-xylene is 9 wt %.

Results and Discussion

Definition of "Polar" and "Apolar" Domains. The P84/water/*p*-xylene ternary system at 25 °C can be divided into polar and apolar domains where the polar domain consists of PEO and water, and the apolar domain consists of PPO and *p*-xylene due to the difference in polarity between PEO and PPO blocks at room temperature.[1,26] From the block compositions of P84 and the known monomer unit volumes of PPO (95.4 Å^3) and PEO (72.4 Å^3),[25] the volume fraction of PPO blocks is estimated to be ~0.60. The apolar volume fraction, f, containing PPO and *p*-xylene and the polar volume fraction, $(1 - f)$, containing PEO and water can be then defined as

$$\begin{aligned} f &= \Phi_o + 0.6\Phi_p \\ 1 - f &= \Phi_w + 0.4\Phi_p \end{aligned} \quad (1)$$

where Φ_p, Φ_o, and Φ_w are the volume fractions of polymer, oil (*p*-xylene), and water, respectively. To calculate the volume fraction of each component, we used mass densities of 1.00, 1.10, 0.86, 0.94, and 1.05 g/mL for H_2O, D_2O, *p*-xylene, *p*-xylene-d_{10}, and P84, respectively.[22]

Subdomain Structures of Lamellar Phase. The SANS intensities of the P84/water/*p*-xylene (40/40/20 wt %) ternary system at the lamellar phase with varying neutron scattering contrasts are shown in Figure 1. While the scattering intensity varies with H_2O content in water, the positions of the first and the second peaks (with a ratio of 1:2) do not change, which indicates that the structure of the lamellar phase remains the same even as the neutron scattering contrast changes, as expected. The invariance of the structure due to the neutron contrast variation was also confirmed by X-ray scattering measurements (Supporting Information). As the H_2O fraction in water increases from 0 to 60 wt %, the SANS intensity of the first Bragg peak initially decreases and, after becoming vanishingly small at 30 wt % H_2O, it increases again. However, the intensity of the second Bragg peak does not change significantly nor vanish even when the first Bragg peak has almost disappeared (at 30 wt % H_2O in water). This clearly indicates that the polar and apolar domains are not homogeneous mixtures of PEO + water and PPO + oil, respectively, because if they were homogeneous mixtures, the relative intensities of scattering peaks would not change with the scattering contrast. In other words, the change of relative peak intensities with the scattering contrast indicates that the polar and apolar domains have subdomain structures.

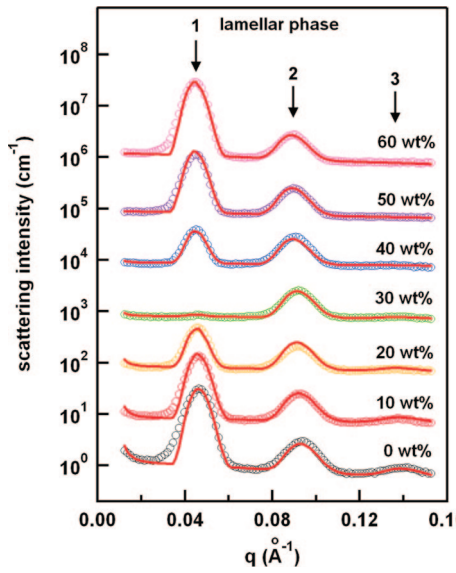

Figure 1. SANS intensities of P84/water/*p*-xylene-d_{10} (40/40/20 wt %) in the lamellar phase with different H_2O weight fractions in water as indicated in the graph. The solid lines are theoretical calculations. The curves are shifted vertically for visual clarity.

To account for the change of relative peak intensities, we modeled the SLD profile as in Figure 2 by introducing three different types of subdomain layers depending on the distribution of solvents: solvent-rich layers, solvent-depleted layers, and homogeneous mixture layers. First, the water-rich layers are assumed in the middle of the polar domains because the PEO blocks protrude from the both sides of the polar/apolar interfaces and terminate near the middle of the polar domains. The oil-rich layers, however, are not considered because some fraction of central PPO blocks is expected to span the whole apolar domain and form a monolayer structure, making fairly homogeneous apolar layers.[1,27] Second, the solvent-depleted layers at the polar/apolar interfaces are included, because the direct contact of water and *p*-xylene at the polar/apolar interfaces is unfavorable due to the high interfacial tension.[18] Lastly, the rest of the subdomains are approximated as homogeneous mixtures of PEO + water and PPO + oil, respectively. The thicknesses of the water-rich layer, water-depleted PEO layer, and oil-depleted PPO layer are denoted as t_w, t_{EO}, and t_{PO}, respectively.

The scattered intensity of a stack of layers is given by[28]

$$I(q) = S(q)|F(q)|^2/q^2 + b \quad (2)$$

where $1/q^2$term is the Lorentz correction factor for randomly oriented stacks and b is the incoherent background. $S(q)$is the structure factor which describes the one-dimensional crystalline order of the lamellae stack, and can be written as follows according to the paracrystalline theory:[29,30]

$$S(q) = N + 2\sum_{k=1}^{k=N-1}(N - k)\cos(kqd)\exp(-k^2q^2\Delta^2/2) \quad (3)$$

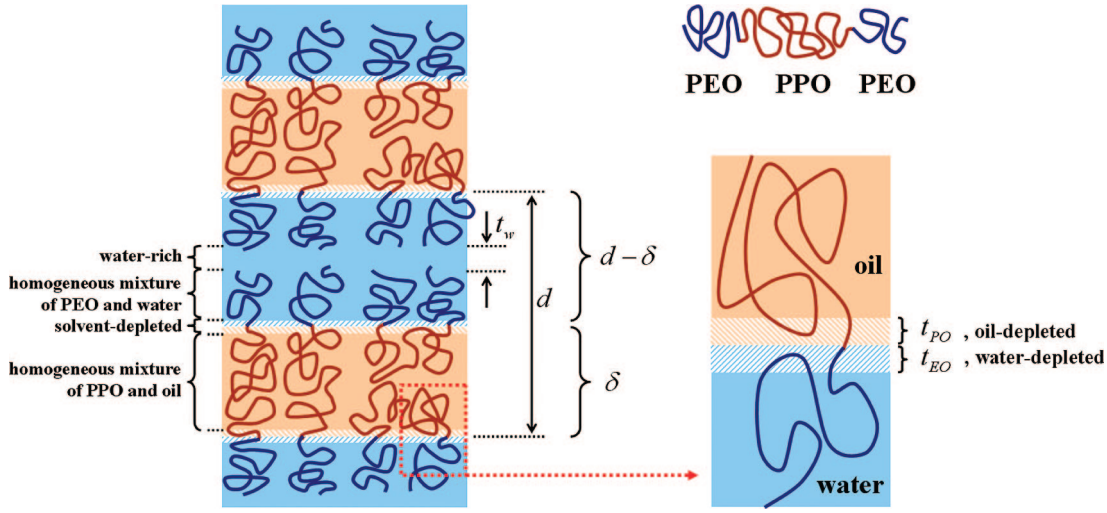

Figure 2. Subdomain structures of the P84/water/*p*-xylene ternary system at lamellar phase. d and δ are the lamellar periodicity and apolar domain thickness, respectively.

where Δ denotes the mean square fluctuations of the layer spacing d. The scattering amplitude $F(q)$ is the Fourier transform of the scattering length density modulation $\rho(z)$ across a single layer spacing d. By taking the center of the apolar layer as the origin, the SLD profile with multiple sublayers as depicted in Figure 2 can be expressed as:

$$\rho(z) = \begin{cases} \rho_{PO+o} & \text{when } 0 \le |z| < t_{PO+o}/2, \\ \rho_{PO} & \text{when } t_{PO+o}/2 \le |z| < t_{PO+o}/2 + t_{PO}, \\ \rho_{EO} & \text{when } t_{PO+o}/2 + t_{PO} \le |z| < t_{PO+o}/2 + t_{PO} + t_{EO}, \\ \rho_{EO+w} & \text{when } t_{PO+o}/2 + t_{PO} + t_{EO} \le |z| < t_{PO+o}/2 + t_{PO} + t_{EO} + t_{EO+w}/2, \\ \rho_{w} & \text{when } t_{PO+o}/2 + t_{PO} + t_{EO} + t_{EO+w}/2 \le |z| \end{cases} \quad (4)$$

where ρ_o, ρ_w, ρ_{PO}, and ρ_{EO} are the SLDs of oil, water, PPO and PEO. ρ_{PO+o}, t_{PO+o} and ρ_{EO+w}, t_{EO+o} represent the SLDs and thicknesses of homogeneously mixed layers of PPO + oil and PEO + water, respectively. The interfaces between the layers may be diffusive but for simplicity it is not included. In this SLD profile, for simplicity it is assumed that the water-rich layer consists of just water and the water- and oil-depleted layers consist of PEO blocks and PPO blocks only, respectively. This may result in a slight underestimation of the thickness of the water-rich layer and the solvent depleted layer, but as will be shown, this model provides an accurate representation of the data. Since $\delta = t_{PO+o} + 2t_{PO}$ and $d - \delta = t_{EO+w} + 2t_{EO} + t_w$, the scattering amplitude can be written as:

$$\begin{aligned} F(q) = {} & (\rho_{PO+o} - \rho_{PO}) \sin(qt_{PO+o}/2) + \\ & (\rho_{PO} - \rho_{EO}) \sin[q(t_{PO+o}/2 + t_{PO})] + \\ & (\rho_{EO} - \rho_{EO+w}) \sin[q(\delta/2 + t_{EO})] + \\ & (\rho_{EO+w} - \rho_{w}) \sin[q(d/2 - t_w/2)] \end{aligned} \quad (5)$$

The SLDs $\rho_{PO+o}$and ρ_{EO+w} are related to the averaged SLDs of the apolar and polar domains $\bar{\rho}_{apolar}$ and $\bar{\rho}_{polar}$ as follows:

$$\begin{aligned} \bar{\rho}_{apolar} &= [t_{PO+o}\rho_{PO+o} + 2t_{PO}\rho_{PO}]/\delta \\ \bar{\rho}_{polar} &= [t_{EO+w}\rho_{EO+w} + 2t_{EO}\rho_{EO} + t_w\rho_w]/(d - \delta) \end{aligned} \quad (6)$$

Therefore, the lamellar periodicity (d) and its mean square fluctuations (Δ), and the thicknesses of water-rich layer (t_w) and solvent-free layers (t_{PO}, t_{EO}) can be obtained by simultaneous fitting of the scattering intensities of seven samples with different neutron contrast using eq 2.

The scattering intensities of the P84/water/*p*-xylene (40/40/20 wt %) ternary systems with different neutron contrast were simultaneously fitted using the model for lamellar phase with subdomain structures (Figure 1). The instrument resolution function was incorporated in the fitting and the incoherent background was fitted individually for the samples with different neutron contrast. It should be noted that the simultaneous model fitting reproduces all the intensity variations (including the relative intensity variations even up to the third order peak) depending on the neutron contrast, remarkably well, resulting in a single set of fitting parameters: a lamellar periodicity (d) of (137.8 ± 2.3) Å with a mean square fluctuation (Δ) of (2.4 ± 0.02) Å, a water-rich layer thickness (t_w) of (5.7 ± 0.06) Å, a water-depleted PEO layer thickness (t_{EO}) of (2.2 ± 0.01) Å, and an oil-depleted PPO layer thickness (t_{PO}) of (4.5 ± 0.01) Å, respectively. The apolar and polar domain thicknesses (δ = 63.4 Å and $d - \delta$ = 74.4 Å, respectively) are calculated from the lamellar periodicity and the apolar volume fraction ($f \sim 0.46$) using the relation $\delta = df$, which is consistent with a previous study.[3] Without the subdomain structures in the polar and apolar domains of lamellar phase, the relative scattering intensity variations with neutron contrast cannot be reproduced at all. Furthermore, if either of the water-rich layer or the water- and oil-depleted layers are not included, the simultaneous fitting could not reproduce all the intensity variations, which strongly indicates the existence of the subdomain structures described in Figure 2.

From the water-rich layer and the polar domain thicknesses, the average end-to-end distance of PEO chains in the lamellar phase is estimated to be 34 Å. Considering that the stretched length of PEO chains for a zigzag conformation is about 67 Å, the PEO chains are not highly stretched as it has been previously reported for different types of Pluronic block copolymers.[2] The thickness of the oil-depleted layer in the polar/apolar interfaces is larger than that of the water-depleted layer. This is consistent with the fact that *p*-xylene, a very hydrophobic oil, is a bad solvent for PEO[18] while water is known to be able to dissolve PPO slightly at room temperature.[1,26] Therefore, it is likely that water can exist closer to the apolar/polar interface than *p*-xylene, which, in our simplified model, can be indicated by smaller t_{EO} than t_{PO}.

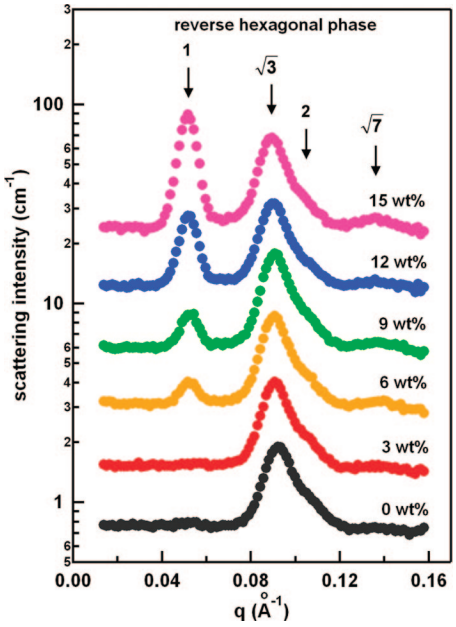

Figure 3. SANS intensities of P84/D_2O/*p*-xylene (46/18/36 wt %) in a reverse hexagonal phase with different hydrogenated *p*-xylene weight fractions in oil as indicated in the graph. The scattering intensities are shifted vertically for visual clarity.

Subdomain Structures of Reverse Hexagonal Phase. The SANS intensities of the P84/water/*p*-xylene (46/18/36 wt %) system in the reverse hexagonal phase with different neutron contrasts show similar behavior as that of the lamellar samples (Figure 3). As the fraction of hydrogenated *p*-xylene in oil increases from 0 to 15 wt %, the intensity of the first Bragg peak initially decreases and, after reaching the minimum at 3 wt % hydrogenated *p*-xylene, it increases again. Again, the intensity of the second Bragg peak does not change significantly nor vanish even when the first Bragg peak has almost disappeared (at 3 wt % hydrogenated *p*-xylene). This, again, clearly indicates that the polar and apolar domains are not homogeneous mixtures of PEO + water and PPO + oil, respectively, but have subdomain structures.

To account for the change of relative peak intensities, we modeled the subdomain structures in a similar way as for the lamellar phase analysis (Figure 4). First, we included a water-rich cylinder core of radius r_w within the polar domain defined by a radius (R), given by the following expression using the lattice parameter a and the apolar volume fraction f,

$$R = a\left(\frac{\sqrt{3}}{2\pi}(1 - f)\right)^{1/2} \tag{7}$$

Second, oil-rich domains are not considered for similar reasons we described for the lamellar structure analysis. Lastly, water- and oil-depleted layers at the polar/apolar interface are included in the model as cylindrical shells with thicknesses of t_{EO} and t_{PO}, respectively.

It is well-known that the powder scattering pattern of an ordered particulate system is described as a multiplication of a form factor and a structure factor (eq 2) and the relative amplitude of scattering peaks is directly dependent on the form factor. Since the peak intensities of the structure factor are the same for the first and second Bragg reflection of a hexagonal packing, the relative intensities of the first and second Bragg peaks of hexagonally packed multishell cylinders are solely described by the form factor of a multishell cylinder. Therefore, we compared the calculated relative intensities of the first and second Bragg peaks determined by the form factor with those

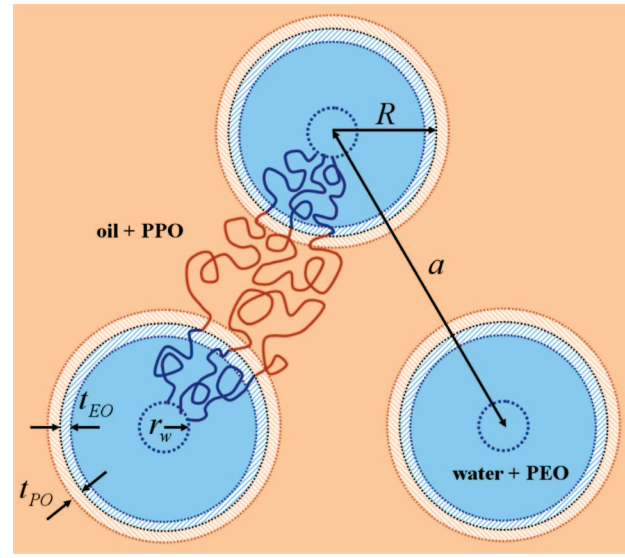

Figure 4. Subdomain structures of the P84/water/*p*-xylene ternary system in a reverse hexagonal phase.

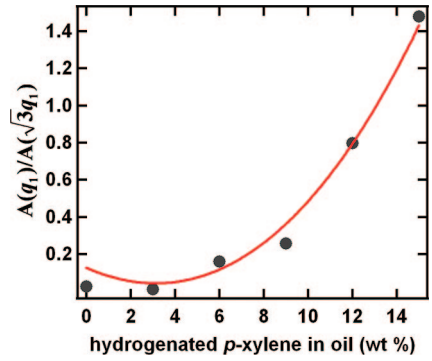

Figure 5. Relative intensity ratios of the first Bragg peaks to the second Bragg peaks determined from contrast varied SANS intensities (solid circles). The fitted curve (solid line) is calculated from the form factor of a multishell cylinder.

observed rather than fitting the entire scattering intensities.[31,32] Since the form factor intensity distribution of a multishell cylinder varies with neutron contrast, the observed ratios of the first and the second order peak intensities, $A(q_1)/A(\sqrt{3}q_1)$, are plotted as a function of the hydrogenated *p*-xylene weight fraction in the oil (Figure 5) where q_1 is the first order Bragg peak position. The theoretical curve is obtained from the calculated form factor ratios of a multishell cylinder at the positions of the first and second Bragg peaks, which will be described below.

We modeled the form factor such that the water-rich core is surrounded by shells of a homogeneous mixture of PEO + water, water-depleted PEO, and oil-depleted PPO, successively, in a homogeneous mixture of PPO + oil (Figure 4). For an anisotropic particle (multishell cylinder), the form factor is calculated by averaging the scattering amplitude over all possible orientations such that:

$$P(q) = \frac{\phi}{v}\int |f_{multishell}(q, \theta)|^2 2\pi \sin\theta \, d\theta \tag{8}$$

where ϕ, v, and $f_{multishell}$ are the volume fraction, volume, and scattering amplitude of the particle, respectively. The scattering amplitude of a multishell cylinder, as depicted in Figure 4, is given as:

$$f_{multishell}(q,\theta) = 2(\rho_w - \rho_{EO+w})V_{core}j_0(qL\cos\theta/2)\frac{J_1(qr_w\sin\theta)}{qr_w\sin\theta} + 2(\rho_{EO+w} - \rho_{EO})V_{EO+w}j_0[q(L/2 + r_w + t_{EO+w})\cos\theta] \times \frac{J_1[q(r_w + t_{EO+w})\sin\theta]}{q(r_w + t_{EO+w})\sin\theta} + 2(\rho_{EO} - \rho_{PO})V_{EO}j_0 \times [q(L/2 + r_w + t_{EO+w} + t_{EO})\cos\theta] \times \frac{J_1[q(r_w + t_{EO+w} + t_{EO})\sin\theta]}{q(r_w + t_{EO+w} + t_{EO})\sin\theta} + 2(\rho_{PO} - \rho_{PO+o})V_{PO}j_0[q(L/2 + R + t_{PO})\cos\theta] \times \frac{J_1[q(R + t_{PO})\sin\theta]}{q(R + t_{PO})\sin\theta} \quad (9)$$

where ρ_w, ρ_{EO+w}, ρ_{EO}, ρ_{PO}, and ρ_{PO+o} are the SLDs of the water-rich core, homogeneous shell of PEO + water, water-depleted PEO shell, oil-depleted PPO shell, and homogeneous domain of PPO + oil, respectively. In this SLD profile, for simplicity it is assumed that the water-rich core consists of just water and the water- and oil-depleted shells consist of PEO blocks and PPO blocks only, respectively. The thickness of the homogeneous PEO + water shell is given by t_{EO+w} such that $R = r_w + t_{EO+w} + t_{EO}$. The volumes of the water-rich core and shells of PEO + water, water-depleted PEO, and oil-depleted PPO are represented by V_{core}, V_{EO+w}, V_{EO}, and V_{PO}, respectively. $j_0(x) = \sin(x)/x$ and $J_1(x)$ is the first order Bessel function. The cylinder length (L) is considered to be very long (practically infinite) throughout the calculation since the scattering peaks represent a 2D hexagonal lattice structure.[31,32] The SLDs ρ_{PO+o} and ρ_{EO+w} are related to the average SLDs of the apolar and polar domains $\bar{\rho}_{apolar}$ and $\bar{\rho}_{polar}$ as follows:

$$\bar{\rho}_{apolar} = [\pi((R + t_{PO})^2 - R^2)\rho_{PO} + (f\sqrt{3}a^2/4 - (\pi(R + t_{PO})^2 - \pi R^2)/2)\rho_{PO+o}]/(f\sqrt{3}a^2/4)$$
$$\bar{\rho}_{polar} = [\pi(R^2 - (R - t_{EO})^2)\rho_{EO} + (\pi(R - t_{EO})^2 - \pi r_w^2)\rho_{EO+w} + \pi r_w^2\rho_w]/\pi R^2 \quad (10)$$

The relative intensity ratios of the first Bragg peaks to the second Bragg peaks, then, can be calculated using eqs 8−10. Here, the form factors (eq 8) should be divided by q^2 to take into account for the Lorenz correction factor, which leads to a multiplication factor of 3. Therefore, the theoretical curve for the relative intensity ratio is obtained by calculating $3P(q_1)/P(\sqrt{3}q_1)$which depends on three parameters: the radius of water-rich core (r_w), thicknesses of the water-depleted PEO shell (t_{EO}), and thickness of the *p*-xylene-depleted PPO shell (t_{PO}), respectively. This fitted ratio is plotted as the solid line in Figure 5.

The model calculation agrees well with the experimentally observed ratios of Bragg peak intensities showing a minimum intensity ratio near 3 wt % of hydrogenated *p*-xylene fraction. The radius of the water-rich core and the thicknesses of water-depleted PEO shell and oil-depleted PPO shell are obtained as (4.4 ± 3.9) Å, (3.6 ± 0.9) Å, and (2.6 ± 0.15) Å, respectively. The polar domain radius (R) is calculated to be 42.3 Å from Eq. 7 using the lattice parameter (a = 137.2 Å) and the apolar volume fraction ($f \sim 0.66$), which is consistent with a previous study.[3]

Without the subdomain structures in the polar and apolar domains of reverse hexagonal phase, the variations of Bragg peak intensity ratio with neutron contrast as in Figure 5 cannot be reproduced at all. Furthermore, if either of the water-rich core or the water- and oil-depleted shells are not included, the theoretical curve as in Figure 5 cannot be reproduced, which strongly indicates the existence of the subdomain structures described in Figure 4.

From the water-rich core and the polar domain radii, the average end-to-end distance of PEO chains is estimated to be 38 Å, which is close to the value obtained from modeling of the lamellar structure (34 Å). The nonzero solvent-depleted layers at the apolar/polar interface have slightly different thickness from the ones obtained in the lamellar sample analysis. This difference may be attributed to the different curvatures at the interface or to the different methods of data analysis for the two systems.

Conclusion

We have investigated the subdomain structures of lamellar and reverse hexagonal phases of the P84/water/*p*-xylene ternary system by contrast varied SANS measurements. In both systems, the observed relative intensities of Bragg peaks changed as the scattering contrast of the samples was varied. While the scattered intensities of the first Bragg peaks were strongly dependent on the weight fraction of the hydrogenated solvent with minima close to predicted contrast match points, the intensities of the second Bragg peaks did not change significantly at any contrast. This variation of the relative peak intensities cannot be explained by simple models where the polar and apolar domains are regarded as homogeneous mixtures of PEO + water and PPO + oil, respectively, in which case the relative intensities of Bragg peaks do not change. The variation of peak intensities observed clearly indicates the existence of subdomain structures in the polar and apolar regions. For both lamellar and reverse hexagonal Pluronic ternary systems, the analysis of the contrast varied SANS intensities with subdomain structure models reproduced the experimental data very successfully, showing that a water-rich layer exists in the middle of the polar domain and water- and oil- depleted layers exist at the polar/apolar interfaces. To our knowledge, this is the first experimental study to identify the subdomain structures of Pluronic ternary systems. We expect that the results obtained here may provide very useful information for the fabrication of various nanoparticles and nanostructured materials where Pluronic ternary systems are used as templates.[8−10,13,33]

Acknowledgment. This work is supported by the Ministry of Education, Science and Technology of Korea through the Basic Atomic Energy Research Institute (BAERI) program, the basic science research program (R01-2008-000-10219-0), and the CNRF project. We thank M.-J. Woo, M.-H. Lee, and H.-S. Kim for their assistance with the X-ray measurements. This work utilized facilities supported in part by the National Science Foundation under Agreement No. DMR-0454672. The mention of commercial products does not imply endorsement by NIST, nor does it imply that the materials or equipment identified are necessarily the best available for the purpose.

Supporting Information Available: Text describing the SANS data analysis of P84/water/*p*-xylene ternary systems at lamellar phase and reverse hexagonal phase with figures showing SANS intensities and tables of parameters for the theoretical calculations shown in the figures. This material is available free of charge via the Internet at http://pubs.acs.org.

References and Notes

(1) Alexandridis, P.; Olsson, U.; Lindman, B. *Macromolecules* **1995**, *28*, 7700–7710.
(2) Svensson, B.; Alexandridis, P.; Olsson, U. *J. Phys. Chem. B* **1998**, *102*, 7541–7548.
(3) Alexandridis, P.; Olsson, U.; Lindman, B. *Langmuir* **1998**, *14*, 2627–2638.
(4) Svensson, M.; Alexandridis, P.; Linse, P. *Macromolecules* **1999**, *32*, 5435–5443.
(5) Zhao, D.; Feng, J.; Huo, Q.; Melosh, N.; Fredrickson, G. H.; Chmelka, B. F.; Stucky, G. D. *Science* **1998**, *279*, 548–552.

(6) Wang, K.; Zhang, W.; Phelan, R.; Morris, M. A.; Holmes, J. D. *J. Am. Chem. Soc.* **2007**, *129*, 13388–13389.
(7) Kruk, M.; Hui, C. M. *J. Am. Chem. Soc.* **2008**, *130*, 1528–1529.
(8) Yang, C.-S.; Awschalom, D. D.; Stucky, G. D. *Chem. Mater.* **2002**, *14*, 1277–1284.
(9) Sakai, T.; Alexandridis, P. *Langmuir* **2004**, *20*, 8426–8430.
(10) Karanikolos, G. N.; Alexandridis, P.; Itskos, G.; Petrou, A.; Mountziaris, T. J. *Langmuir* **2004**, *20*, 550–553.
(11) Niesz, K.; Grass, M.; Somorjai, G. A. *Nano Lett.* **2005**, *5*, 2238–2240.
(12) Tao, F.; Guan, M.; Jiang, Y.; Zhu, J.; Xu, Z.; Xue, Z. *Adv. Mater.* **2006**, *18*, 2161–2164.
(13) Karanikolos, G. N.; Law, N.-L. V.; Mallory, R.; Petrou, A.; Alexandridis, P.; Mountziaris, T. J. *Nanotechnology* **2006**, *17*, 3121–3128.
(14) Guzman, M.; Garcia, F. F.; Molpeceres, J.; Aberturas, M. R. *Int. J. Pharm.* **1992**, *80*, 119–127.
(15) Kabanov, A. V.; Batrakova, E. V.; Melik-Nubarov, N. S.; Fedoseev, N. A.; Dorodnich, T. Y.; Alakhov, V. Y.; Chekhonin, V. P.; Nazarova, I. R.; Kabanov, V. A. *J. Controlled Release* **1992**, *22* (2), 141–157.
(16) Discher, D. E.; Eisenberg, A. *Science* **2002**, *297*, 967–973.
(17) Alexandridis, P.; Olsson, U.; Lindman, B. *J. Phys. Chem.* **1996**, *100*, 280–288.
(18) Holmqvist, P.; Alexandridis, P.; Lindman, B. *Macromolecules* **1997**, *30*, 6788–6797.
(19) Svensson, B.; Olsson, U.; Alexandridis, P. *Langmuir* **2000**, *16*, 6839–6846.
(20) Pedersen, J. S.; Gerstenberg, M. C. *Colloids Surf. A* **2003**, *213*, 175–187.
(21) Lettow, J. S.; Lancaster, T. M.; Glinka, C. J.; Ying, J. Y. *Langmuir* **2005**, *21*, 5738–5746.
(22) Svensson, B.; Olsson, U.; Alexandridis, P.; Mortensen, K. *Macromolecules* **1999**, *32*, 6725–6733.
(23) Glinka, C. J.; Barker, J. G.; Hammouda, B.; Krueger, S.; Moyer, J. J.; Orts, W. J. *J. Appl. Crystallogr.* **1998**, *31*, 430.
(24) Kline, S. R. *J. Appl. Crystallogr.* **2006**, *39*, 895–900.
(25) Chen, S. H.; Liao, C.; Fratini, E.; Baglioni, P.; Mallamace, F. *Colloids Surf. A* **2001**, *183*−*185*, 95–111.
(26) Alexandridis, P.; Nivaggioli, T.; Hatton, T. A. *Langmuir* **1995**, *11*, 1468–1476.
(27) Hecht, E.; Mortensen, K.; Hoffmann, H. *Macromolecules* **1995**, *28*, 5465–5476.
(28) Nallet, F.; Laversanne, R.; Roux, D. *J. Phys. II* **1993**, *3*, 487–502.
(29) Blaurock, A. E. *Biochim. Biophys. Acta.* **1982**, *650*, 162–207.
(30) Pabst, G.; Koschuch, R.; Pozo-Navas, B.; Rappolt, M.; Lohner, K.; Laggner, P. *J. Appl. Crystallogr.* **2003**, *36*, 1378–1388.
(31) Ramos, L.; Fabre, P.; Ober, R. *Eur. Phys. J. B* **1998**, *1*, 319–326.
(32) Krishnaswamy, R.; Pabst, G.; Rappolt, M.; Raghunathan, V. A.; Sood, A. K. *Phys. Rev. E* **2006**, *73*, 031904.
(33) Zhang, R.; Liu, J.; He, J.; Han, B.; Wu, W.; Jiang, T.; Liu, Z.; Du, J. *Chem. Eur. J.* **2003**, *9*, 2167–2172.

MA802296U